ROUGHNESS EFFECTS OF TEXTURED SURFACES IN HYDRODYNAMIC LUBRICATION

Youssef BAHI[*]
Moulay Ismail University Faculty of Science FS-Meknes, MOROCCO
Research Laboratory in Advanced Materials and Applications – LEM2A
E-mail: y.bahi@ensam-umi.ac.ma

Mhammed El GADARI
Moulay Ismail University High School of Engineering ENSAM Meknes, MOROCCO
Research Laboratory in Mechanical Engineering, Mechatronics & Control – L2MC

Miloud RAHMOUNE
Moulay Ismail University Faculty of science FS-Meknes, MOROCCO
Research Laboratory in Advanced Materials and Applications – LEM2A

Several studies have been conducted to improve and model the lubricated contact between surfaces. The main subjects were defining the hydrodynamic parameters to reduce energy losses and protect the environment. Some of the proposed models have studied the effect of textures in hydrodynamic lubrication and have proved that adapted shapes and geometries can improve the performance of lubricated contacts. A hydrodynamic model was developed by assuming the roughness of the textured surface and considering the cavitation in a steady-state regime. The proposed model was validated and compared with the analytical model of Fowell *et al.* [1]. Three different textures shapes were considered. The results showed that the rough-textured thrust affects the hydrodynamic performance significantly. Thus, by increasing the arithmetic roughness of textured surfaces, the hydrodynamic pressure, and the lifting force increase depending on the texture shape. A rougher surface slightly increases the friction force for the three considered textures.

Keywords: finite difference, texture, roughness, HD pressure, lifting force, friction, leakage.

1. Introduction

The wear reduction between interacting surfaces has been the most relevant research issue in the latest decades (Holmberg and Erdemir [2]). This contact is defined by several tribological parameters: temperature, elasticity, surface finish, and film rheology.

It is well known that textured surfaces improve hydrodynamic performance significantly. However, the surface roughness could generate dry contact between asperities in lubricated contact. It is important to note that the surface textures are obtained by physical or chemical processes.

The technique of surface texturing is known as a technological solution to reduce friction and wear in engines. It is widely used to improve performance in the hydrodynamic mixed or limit lubrication regime (Sudeep [3], Gu [4]).

Regarding the numerical simulation of the texture system, since the lubricant film generates several ruptures and replenishment, it is generally accepted that a cavitation mass conservation treatment is required to obtain an accurate performance (Ausas *et al.* [5]). Therefore, mass conservation models based on the JFO cavitation boundary conditions (Jakobsson [6], Olsson [7]) are experimentally validated and most used in the literature (Gropper *et al.* [8]).

---

[*] To whom correspondence should be addressed

Generally, the effect of roughness is neglected in hydrodynamic models of textured surfaces. However, experimental studies have demonstrated that rough surfaces affect the lubricated contact performance.

This paper presents a numerical model designed by considering the geometrical and tribological characteristics of the surfaces, such as texture and roughness, and the problem of cavitation of the lubricant film. A parametric study will be carried out to determine the impact of the above factors.

2. Validation of the hydrodynamic model

To validate the hydrodynamic model based on the finite difference method a comparison between the numerical results and the analytical model by (Fowell [1], Tauviqirrahman [9]) was made.

Hence, the case of a textured thrust (Fig.1), where the surface is represented by a singular cavity. For hydrodynamic lubrication, the governing equation is described by the famous Reynolds equation. The following assumptions are used in the Reynolds approach:

- low film thickness compared to the contact width dimension,
- incompressible fluid,
- laminar flow,
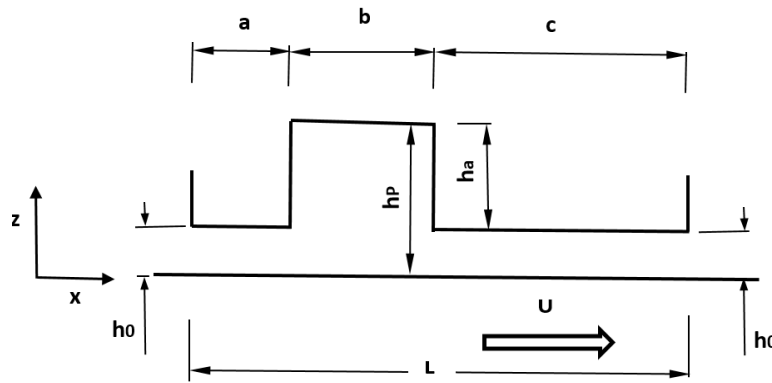- gravitational forces are neglected compared to the viscous force.

Fig.1. Schematic of the textured thrust.

The numerical values for the geometry and operational parameters are listed in the table below:

Table 1. The geometry and operational conditions of the thrust.

Contact length	L	20 mm
Length entry	a	4 mm
Pocket length	b	6 mm
Output length	c	10 mm
Minimal film thickness	h_0	1 micron
Pocket depth	h_a	5 microns
velocity	U	1 m/s
Dynamic viscosity	μ	0.01 Pa s
Ambient pressure	p_0	0.1 MPa
Cavitation pressure	p_{cav}	0 MPa

2.1. Numerical model

Governing equations

To compute the hydrodynamic performances: the frictional force, lifting force, leakage rate, and cavitated area, the modified Reynolds equation is used according to the formulation of El Gadari and Hajjam [10]:

$$F\frac{\partial}{\partial x}\left(h^3\frac{\partial D}{\partial x}\right)=6\mu U\frac{\partial h}{\partial x}+6\mu(1-F)\left(U\frac{\partial D}{\partial x}\right) \tag{2.1}$$

where: D is a universal variable and F is the cavitation index

$$D=p \quad \text{and} \quad F=1. \quad \text{when} \quad D>0,$$

$$D=r-h, \quad r=\left(\frac{\rho}{\rho_0}\right)h, \quad p=p_{cav} \quad \text{and} \quad F=0 \quad \text{when} \quad D\le 0$$

ρ and ρ_0 are, respectively, the densities of the lubricant-gas mixture and lubricant, r is the rate of replenishment, p is the hydrodynamic pressure of the lubricating oil, h is the thickness of the film in the contact

$$h(x)=h_0 \quad \text{for} \quad 0\le x\le a \quad \text{and} \quad a+b\le x\le L,$$

$$h(x)=h_0+h_a \quad \text{for} \quad a\le x\le a+b,$$

U is the translational velocity, μ is the dynamic viscosity of the lubricant, D at $x=0$ is equal to the atmospheric pressure p_0, and at $x=L$, D is equal to operating pressure $p=p_0$.
Consequently, the Reynolds equation is solved to identify the hydrodynamic pressure distribution along the contact width, and then:

- the lifting force:

$$W=\int_0^L (p-p_0)dx, \tag{2.2}$$

- the shearing rate:

$$\tau_{xz}=-F\left(\frac{U\mu}{h}+\frac{h}{2}\frac{\partial p}{\partial x}\right)-(1-F)\frac{r}{h}\frac{U\mu}{h}, \tag{2.3}$$

- friction force:

$$F_f=\int_0^L \tau_{xz}dx, \tag{2.4}$$

- flow rate:

$$Q = -\frac{h^3}{12\mu}\frac{\partial p}{\partial x} + \frac{Uh}{2}.$$ (2.5)

Numerical solution

A finite-difference approach is performed based on an approximation of the differential operators from the Taylor series. This approach is still widely used in lubricated contact simulation due to its simplicity. The figure below describes the domain meshing.
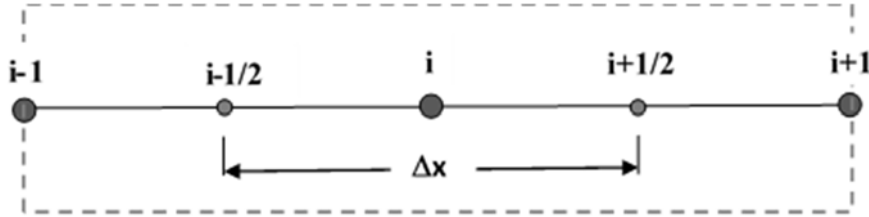

Fig.2. Representation of the discretization model

The Reynolds equation in discretized form is written:

$$A(i,i+1)D(i+1) + A(i,i)D(i) + A(i,i-1)D(i-1) = B(i)$$ (2.6)

with

$$A(i,i+1) = \left(\frac{h(i)^3 + h(i+1)^3}{2(\Delta x)^2}\right)F(i+1),$$ (2.7)

$$A(i,i) = -\left(\frac{h(i+1)^3 + 2*h(i)^3 + h(i-1)^3}{2(\Delta x)^2}\right)F(i) - 6\mu U\frac{(1-F(i))}{\Delta x},$$ (2.8)

$$A(i,i-1) = \left(\frac{h(i)^3 + h(i-1)^3}{2(\Delta x)^2}\right)F(i-1) - 6\mu U\frac{(1-F(i-1))}{\Delta x},$$ (2.9)

$$B(i) = 6\mu U\left(\frac{h(i) - h(i-1)}{\Delta x}\right).$$ (2.10)

2.2. Analytical model

The mortality method used in the Reynolds equation developed at thrust of the surface is similar to Fowell's study [1]. The following analysis is based on mass conservation. The area between B and B' represents the cavitation zone obtained further in this paper.
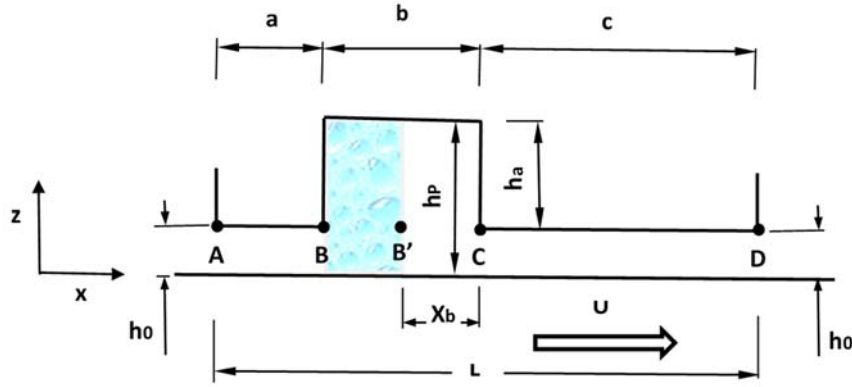
Fig.3. Film interaction for the analytical model.

Based on the Reynolds equation of the first order, the flow rate is given:

$$q(x) = -\frac{h^3}{12\mu}\frac{\partial p}{\partial x} + \frac{Uh}{2},$$

(2.11)

under the following boundary conditions: $p_A = p_0$; $p_B = p_{cav}$; $p_{B'} = p_{cav}$; $p_D = p_0$.

Applying Eq.(2.11) in the non-cavitated area yields the following equations:

- between A and B:

$$q_{AB} = -\frac{h_0^3}{12\mu}\frac{(p_{cav} - p_0)}{a} + \frac{Uh_0}{2},$$

(2.12)

- between B' and C:

$$q_{B'C} = -\frac{h_p^3}{12\mu}\frac{(p_C - p_{cav})}{X_b} + \frac{Uh_p}{2},$$

(2.13)

- between C and D:

$$q_{CD} = -\frac{h_0^3}{12\mu}\frac{(p_0 - p_C)}{c} + \frac{Uh_0}{2},$$

(2.14)

In the cavitation zone, the pressure is constant and equal to p_{cav}. The fluid film does not completely occupy the height. Thus, the flow rate is expressed as follows:

$$q_{BB'} = \frac{Urh_p}{2}$$

(2.15)

where: $h_p = h_0 + h_a$.

The preservation of the flow rate means that the above expressions are equalized. This yields the pressure at point C and the width of the non-cavity zone BB':

$$p_C = p_0 - \frac{c}{a}(p_{cav} - p_0),\tag{2.16}$$

$$X_b \frac{h_p^3(p_C - p_{cav})}{6\mu U(h_p - h_0) - h_0^3\left(\dfrac{p_0 - p_{cav}}{a}\right)}.\tag{2.17}$$

The pressure distribution is considered linear throughout the contact. Thus, we can deduce the following expressions:

$$p(x) = \begin{cases} -\left(\dfrac{p_0 - p_{cav}}{a}\right)x + p_0 & x \in [0,a], \\[2mm] p_{cav} & x \in \left[a,(a+b) - X_b\right], \\[2mm] \left(\dfrac{p_C - p_{cav}}{X_b}\right)x + p_C - \left(\dfrac{p_C - p_{cav}}{X_b}\right)(a+b) & x \in \left[(a+b) - X_b,(a+b)\right], \\[2mm] \left(\dfrac{p_0 - p_C}{c}\right)x + p_0 - \left(\dfrac{p_0 - p_C}{c}\right)L & x \in \left[(a+b),L\right]. \end{cases}\tag{2.18}$$

2.3. Numerical results

The numerical and analytical calculations allowed us to determine the pressure distribution within the lubricated contact (Fig.4.):
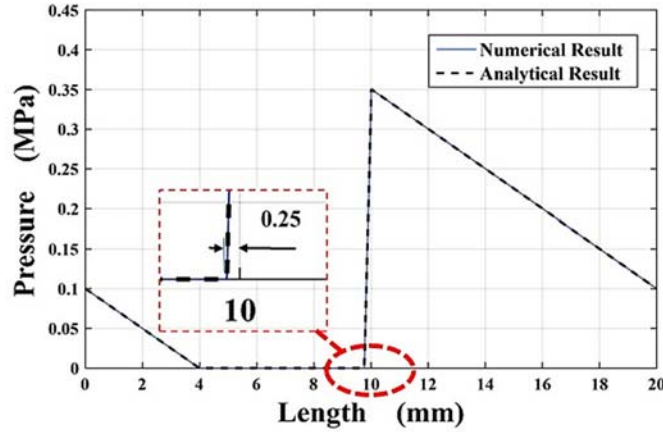

Fig.4. Pressure distribution along the contact length.

Comparing the simulation results and analytical solution of the maximum pressures and the cavitated zone length, good agreement is confirmed for both methods. Consequently, the proposed numerical model is validated.

Subsequently, a parametric study is performed by varying the shapes of the textures and the average roughness. Three textures shapes are studied: rectangular, triangular, and elliptical.

3. Roughness effect on contact performances

The parametric study investigates the rough textured surface effect on the hydrodynamic lubrication performance. For this purpose, three texture shapes are considered, each composed of three pockets. The average roughness of the textured part is taken as equal to *10 nm*, and the arithmetic roughness is varied from *0* to *400 nm* concerning the non-textured area. A comparison will be made based on the support load, frictional force, flow rate, and cavitation rate.

The roughness of the textured and non-textured surface is modeled with a randomized signal $r(x)$ (Fig.5.), and its arithmetic roughness Ra has been analyzed, such as:

$$Ra = \frac{1}{L}\int_0^L |r(x)| dx \qquad (3.1)$$
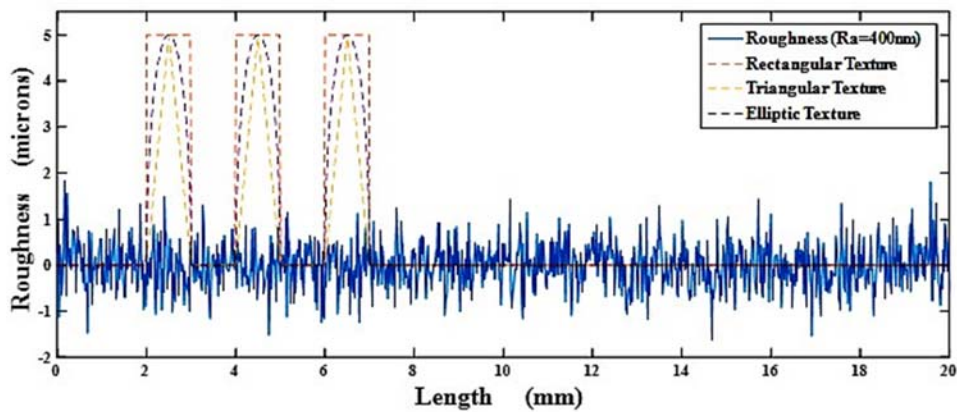
Fig.5. The roughness of non-textured surfaces (Ra = *400* nm).

3.1. Rectangular textures

Three rectangular pockets are made on the fixed thrust (Fig.6.). The shape is described by a depth of $h_a = 5\,microns$, a width $b = 1mm$, and space of $a = 1mm$. ($h_0 = 2\,microns$).
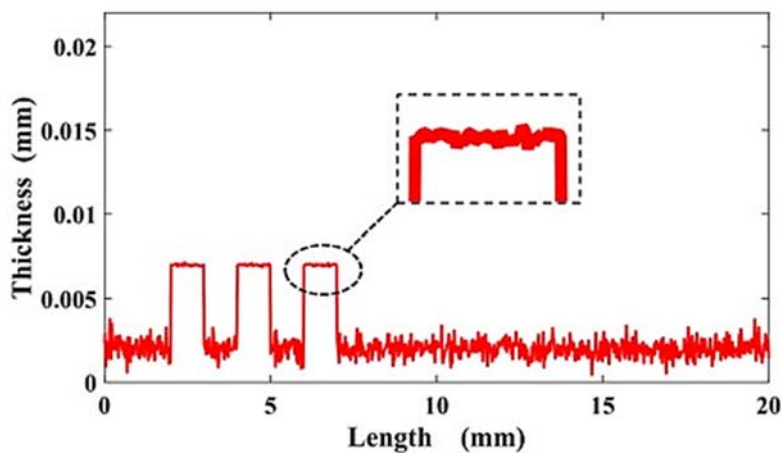

Fig.6. The thrust surface with rough rectangular textures.

Solving the Reynolds equation by the Difference finite approach leads to the pressure variation within the contact. In Fig.7, The hydrodynamic pressure is plotted versus four values of roughness.
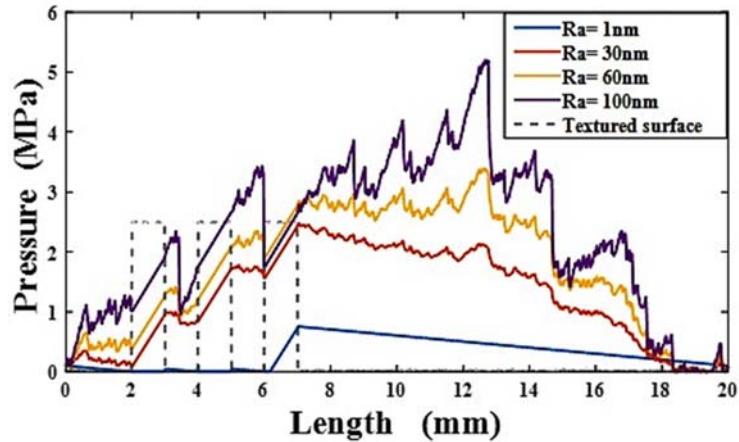

Fig.7. Pressure distribution for four roughness values (rectangular textures).

Figure 7 confirms that when the arithmetic roughness of the non-textured area increases, a substantial jump of the hydrodynamic pressure is induced in the non-textured area compared to the smooth cases. Also, the figure shows that cavitation occurs for smooth textures in the convergent-divergent area, contrary to the case of the rough texture, where the non-active area is located in the vicinity of the external side.

3.2. Triangular textures

The second case proposes to study triangular textures of height $h_a = 5\,microns$ and base $b = 1mm$, a distance of $a = 1mm$ ($h_0 = 2\,microns$).
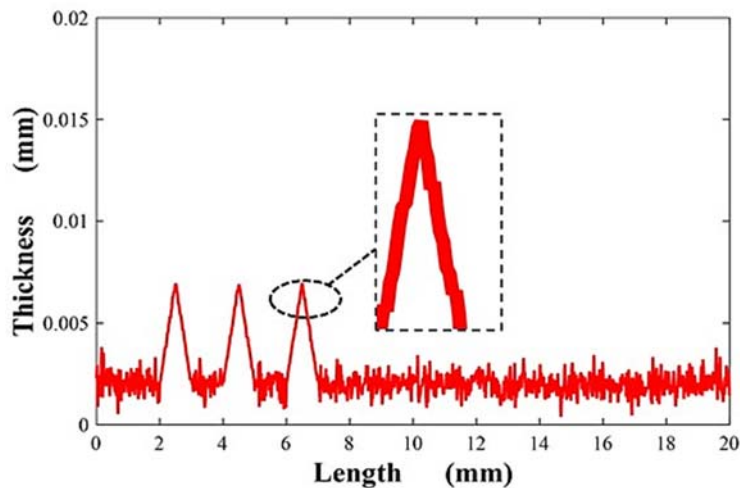

Fig.8. The thrust surface with rough triangular textures.

As in the previous case, the pressure distribution is presented along a surface with triangular textures considering four roughness values:
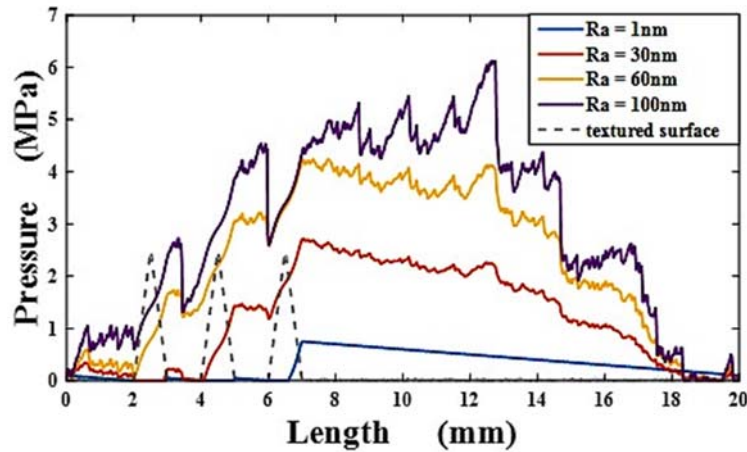
Fig.9. Pressure distribution for four roughness values (triangular textures).

Figure 9 demonstrates that the hydrodynamic pressure is strongly impacted by the arithmetic roughness and increases with rougher surfaces. Also, it is relevant to underline that the triangular textures coupled with surface roughness increase the cavitated area compared to rectangular textures. Indeed, for triangular textures with a low roughness surface, cavitation occurs at the exit of the lubricated contact, but also in the vicinity of smooth of the convergent-divergent areas.

3.3. Elliptic textures

The third shape is an elliptical texture of height $h_a = 5\,microns$, large-diameter $b = 1mm$. The three textures are distant by $a = 1mm$ ($h_0 = 2\,microns$).
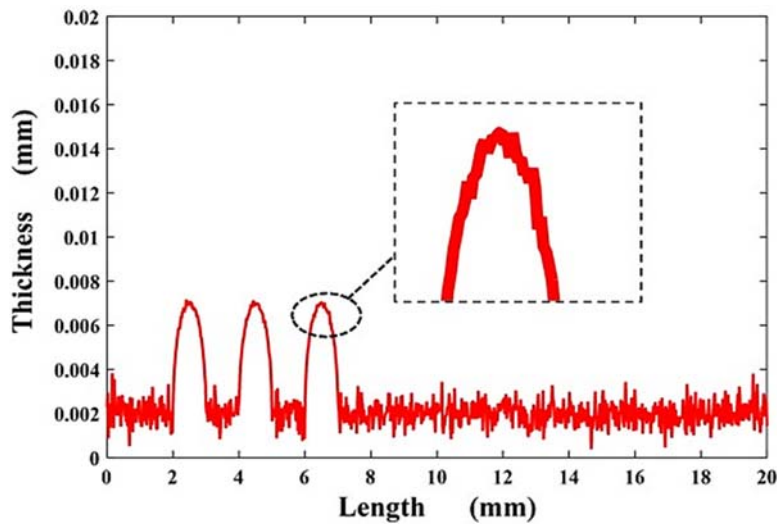

Fig.10. The thrust surface with rough elliptical textures.

With elliptical textures made on the fixed surface, the hydrodynamic pressure will be distributed, for different roughness values, as follows:
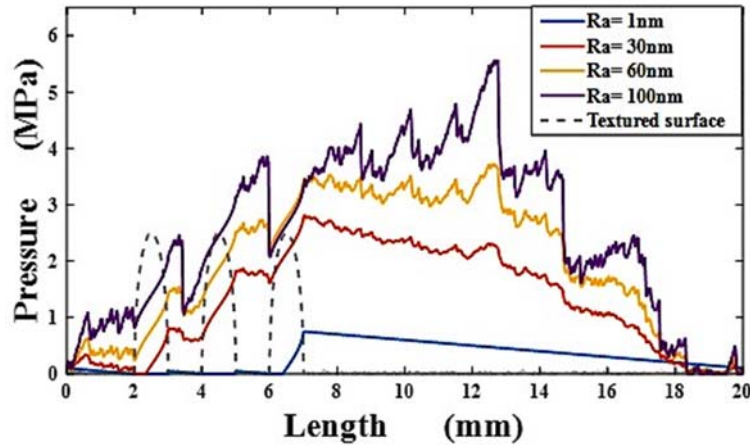
Fig.11. Pressure distribution for four roughness values (elliptical textures).

Figure 11 confirms that the hydrodynamic pressure increases with the arithmetic roughness of the textured surfaces. Indeed, the rough elliptical textures generate a hydrodynamic pressure $p_{max} = 5.5 MPa$ similar to that generated by rough rectangular textures, but relatively low compared to rough triangular textures $p_{max} = 6.3 MPa$.

3.4. Comparison between tribological performances: flow, load support, friction

The figures below demonstrate the evolution of tribological parameters: lifting force, friction, and flow as a function of the average roughness of the non-textured area for the different textures mentioned above.
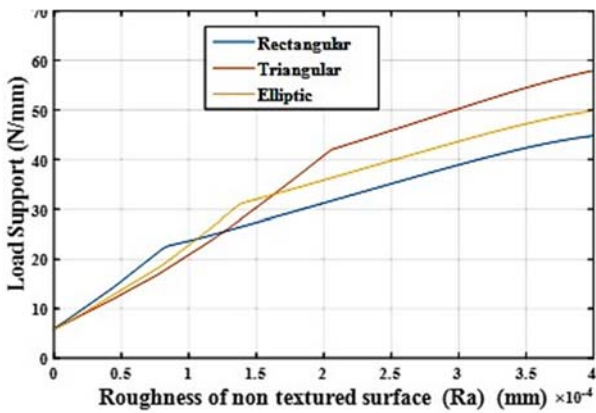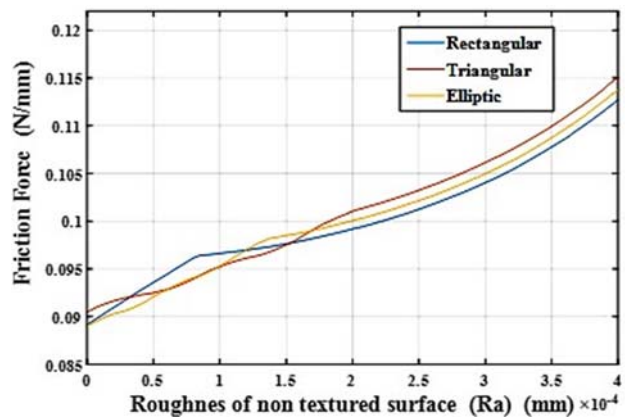

Fig.12. Lifting force.

Fig.13. Friction force.

Figure 12 shows that the load support increases proportionally to the arithmetic roughness of the non-textured area. Additionally, over a specific value (*0.08*, *0.14*, and *0.2 microns* for rectangular, elliptical, and triangular textures respectively), the lifting force gradient is reduced.

Figure 12 also shows that rough triangular textures generate *20%* more load support compared to rough elliptical textures and *40%* difference with rectangular textured surfaces.

Figure 13 shows that the viscous friction increases almost proportionally to the arithmetic roughness of the non-textured area. Moreover, beyond a roughness value (*0.08*, *0.14*, and *0.2 microns*), the gradient of friction increase becomes smaller. It should be noted that while the lifting force depends on the types of rough textures, the viscous frictional force remains the same for the three types of rough-textured surfaces.
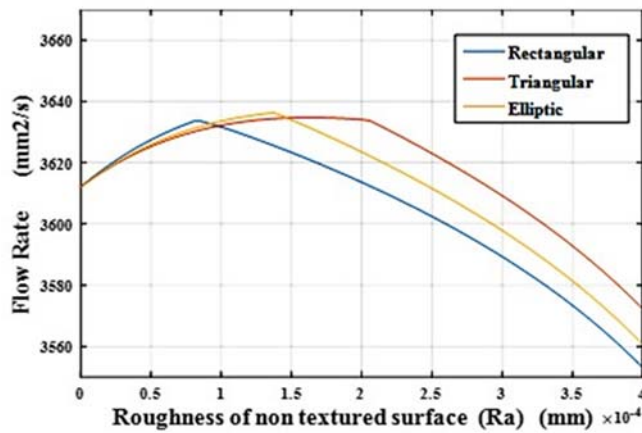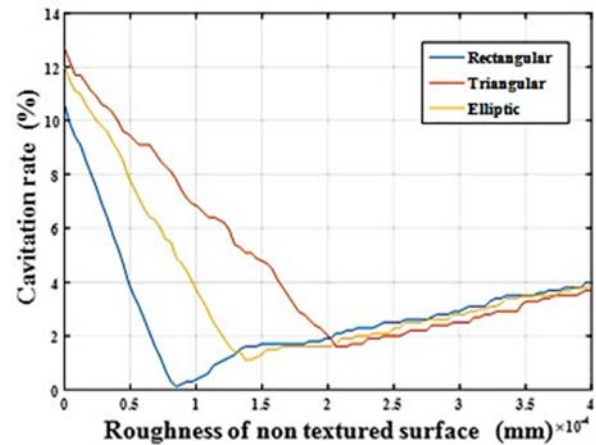
Fig.14. Flow rate.

Fig.15. Cavitation rate.

According to Fig.14, the flow rate has a parabolic shape as a function of the arithmetic roughness of the non-textured area. Moreover, from the values $Ra = 0.08, 0.14$ and $0.2\ microns$, for the rectangular, elliptical, and triangular textures, respectively, the flow rate has a maximum value. In addition, rough rectangular textures generate a very low flow rate compared to the other two types of textures with a very important difference from the case of rough triangular textures.

The graph shown in Fig.15 illustrates how the roughness can affect the cavitation rate for the three textures. It is clearly seen that an increase in the arithmetic value of the roughness can considerably reduce the percentage of cavitated areas. Also, from specific values, the latter stabilizes between *2%* and *4%* for each type of texture.

4. Conclusion

In the present work, the hydrodynamic model is validated by comparing numerical results with the analytical solution given by Fowell *et al.* [1]. Then, a parametric study is conducted to investigate the effects of roughness on the performance of a lubricated contact between a thrust and a smooth shaft. Three different texture shapes (rectangular, triangular, and elliptical) are performed on the thrust surface, considering a low roughness on the textured part and different roughnesses on the non-textured areas. Simulations showed that an increase in the arithmetic roughness of the non-textured part leads to an increase in the hydrodynamic pressure. The latter becomes higher for triangular textures. In addition, the load support increases proportionally to the arithmetic roughness of the non-textured area. Also, beyond a specific value, the gradient of the lifting force decreased. Thus, the triangular textures produce a substantial lifting force. In addition, the flow rate varies as a parabolic function versus the roughness, and above a specific arithmetic roughness the flow decreases.

As the shaft roughness was not considered, we in the nearest future intend to investigate the roughness effect of the textured surfaces for more complex cases: the shaft roughness, the surface's elasticity, and the thermal effect.

Acknowledgements

Nomenclature

D – universal variable
F – cavitation index
F_f – friction force [*N/mm*]
h – film thickness [*micron*]
h_0 – minimal film thickness [*micron*]
h_a – pocket depth [*micron*]
L – length contact zone [*mm*]
L – speed of shaft surface [*mm/s*]
p – film pressure $[MPa]$
p_s – service pressure $[MPa]$
p_0 – ambient pressure $[MPa]$
p_{cav} – cavitation pressure $[MPa]$
Q – flow rate [*mm²/s*]
r – effective film thickness (replenishment ratio) [*mm*]
W – load support [*N/mm*]
μ – viscosity of the lubricant $[MPa\,s]$
ρ – lubricant density $\left[kg/m^3\right]$
τ_{xy} – shearing film $[MPa]$

Appendixes

The finite difference approximation of the terms of the Reynolds equation:

$$\frac{\partial}{\partial x}\left(h^3\frac{\partial}{\partial x}(FD)\right)_i = \frac{h\left(i+\frac{1}{2}\right)^3\frac{\partial(FD)}{\partial x}\left(i+\frac{1}{2}\right)-h\left(i-\frac{1}{2}\right)^3\frac{\partial(FD)}{\partial x}\left(i-\frac{1}{2}\right)}{\Delta x},$$

$$\frac{\partial(FD)}{\partial x}\left(i+\frac{1}{2}\right)=\frac{F(i+1)D(i+1)-F(i)D(i)}{\Delta x},$$

$$\frac{\partial(FD)}{\partial x}\left(i-\frac{1}{2}\right)=\frac{F(i)D(i)-F(i-1)D(i-1)}{\Delta x},$$

$$h(i+1/2)^3=\frac{h(i)^3+h(i+1)^3}{2},$$

$$h(i-1/2)^3 = \frac{h(i)^3 + h(i-1)^3}{2}$$

$$\frac{\partial h}{\partial x}(i) = \frac{h(i) - h(i-1)}{\Delta x},$$

$$\frac{\partial((1-F)D)}{\partial x}(i) = \frac{(1-F(i))D(i) - (1-F(i-1))D(i-1)}{\Delta x}$$

References

[1] Fowell M., Olver A.V., Gosman A.D., Spikes H.A. and Pegg I. (2007): *Entrainment and inlet suction: two mechanisms of hydrodynamic lubrication in textured bearings.*– ASME Journal of Tribology, vol.129, pp.336-345.

[2] Holmberg K. and Erdemir A. (2017): *Influence of tribology on global energy consumption, costs and emissions.*– Friction, vol.5, pp.263-284.

[3] Sudeep U., Tandon N. and Pandey RK. (2015): *Performance of lubricated rolling/sliding concentrated contacts with surface textures*: a review.– J Tribol-Trans ASME, vol.137, No.3, Article No.031501, p.11, https://doi.org/10.1115/1.4029770.

[4] Gu C.X, Meng X.H, Xie Y.B. and Yang Y.M. (2016): *Effects of surface texturing on ring/liner friction under starved lubrication.*– Tribology International, vol.94, pp.591-605, https://doi.org/10.1016/j.triboint.2015.10.024.

[5] Ausas R., Ragot P., Leiva J., Jai M., Bayada G. and Buscaglia G.C. (2007): *The impact of the cavitation model in the analysis of microtextured lubricated journal bearing.*– J Tribol-Trans ASME, vol.129, No.4, pp.868-875, https://doi.org/10.1115/1.2768088.

[6] Jakobsson B. and Floberg L. (1957): *The Finite Journal Bearing, Considering Vaporization.*– Gumperts Förlag, p.116.

[7] Olsson K.-O. (1965): *Cavitation in Dynamically Loaded Bearing.*– Scandinavian University Books, p.59.

[8] Gropper D., Wang L. and Harvey T.J. (2016): *Hydrodynamic lubrication of textured surfaces: a review of modeling techniques and key finding.*– Tribology International, vol.94, pp.509-529, https://doi.org/10.1016/j.triboint.2015.10.009.

[9] Muchammad M., Tauviqirrahman M., Jamari J. and Schipper D.J. (2016): *An analytical approach on the tribological behavior of pocketed slider bearings with boundary slip including cavitation.*– Lubrication Science, vol.29, No.3, pp.133-152, https://doi.org/10.1002/ls.1361.

[10] El Gadari M., Fatu A. and Hajjam M. (2016): *Effect of the grooved shaft on the rotary lip seal performance in transient condition: Elasto-hydrodynamic simulation.*– Tribology International, vol.93, Part A, pp.411-418, https://doi.org/10.1016/j.triboint.2015.09.031.